Neutron Resonance Spectroscopy. VII. Ti, Fe, and Ni

J. B. Garg*
State University of New York, Albany, New York 12203
and
J. Rainwater and W. W. Havens, Jr.†
Columbia University, New York, New York 10027
(Received 29 January 1971)

High-resolution neutron total cross-section measurements were performed on natural samples of titanium, iron, and nickel from 200 eV to a few MeV using the Nevis synchrocyclotron neutron velocity spectrometer with a 200-m flight path. The energy resolution was adequate only up to 200 keV to perform a detailed R-matrix multilevel analysis of the data. The resonance energies, isotopic and l-value assignment, neutron widths, etc., up to this energy have been determined. From these the mean level spacings $\langle D\rangle$ and the s-wave strength functions (S_0) have been calculated. Information about the resonance parameters of the bound level in iron and nickel has been also obtained. Values of $\Gamma_\gamma = 8.2$ eV for the Ti^{48} (17.8 keV) resonance, $\Gamma_\gamma = 0.64$ for the bound level at -2 keV in Fe^{56}, and $\Gamma_\gamma = 9.0$ eV for the bound level at -28.5 keV in Ni^{58} have been determined by requiring an agreement with the measured thermal-neutron-capture cross section in these nuclei.

I. INTRODUCTION

The measurement of the total neutron cross section of a nucleus as a function of incident neutron energy provides information on the level energies of the compound nuclei formed in the capture and scattering of the incident neutrons by target nuclei. From these measurements, plus those such as the partial cross sections as a function of energy for radiative capture (n,γ), elastic scattering (n,n), and, where present, fission (n,f) or other reactions, has come our present understanding of the physics involved. The compound-nucleus excitation energy is about 8 MeV above the ground state and a few MeV above the low-lying excited states which are more simply interpreted in terms of shell-model or collective-model states. Considerable emphasis for these highly excited states is placed on the statistical properties of the nuclear states and on the reaction mechanisms. One is concerned with average level spacings, the laws governing the distribution of level spacings, the mean value of the reduced neutron width $\langle\Gamma_n^0\rangle$ (for $l=0$ neutrons), and of the capture width Γ_γ (or of the partial widths $\Gamma_{\gamma j}$; to particular final states j), and the partial widths for other neutron-induced reactions which may occur. One is also interested in the distribution laws followed in the variation of these partial widths about their mean values, and in possible correlations (covariance) in the fluctuations of the various parameters about their mean values for a set of energy levels.

Long-range systemmatic fluctuations of various reaction strengths as a function of the neutron energy and of the size of the target nucleus (atomic charge Z and mass A) were first extensively demonstrated by the fast-neutron studies of Barshall *et al.*[1] These results were interpreted by Feshbach, Porter, and Weisskopf[2] on an "optical-model" basis by treating the "average" (over resonances) neutron-nucleus interaction in terms of a one-body problem with the nucleus treated as a region of complex interaction potential which disturbs the incident neutron wave. The real part of the interaction represents an averaging effect of the nuclear forces on the incident neutron. The imaginary part of the potential relates to the mean free path of the incident neutron in nuclear matter for processes other than prompt "potential scattering." The latter include prompt inelastic or reaction processes and compound-nucleus formation.

The pioneering optical-model paper of Feshbach, Porter, and Weisskopf[2] was successful in duplicating many of the observed experimental features in a qualitative manner. It has been evident from the start, however, that the early calculations were based on an oversimplified model of uniform-density spherical nuclei having sharp edges, with $r = r_0 A^{1/3}$, and with a constant real-plus-imaginary neutron-nucleus interaction potential inside. It was also obvious from the beginning that one should, in principle, use as realistic a model as possible so as to: (a) attempt to include the known information concerning the deviation from spherical shape of each specific target nucleus rather than use a spherical shape; (b) attempt to include as well as possible known information concerning nuclear "edge-thickness" effects, i.e., the variation of $\rho(r,\theta,\phi)$ as suggested by electron scatter-

ing experiments and muonic x-ray studies; (c) attempt to test properly the radial dependence of the potential.

In addition, there has been renewed interest in investigating "intermediate-structure," or "doorway-state" effects which modulate the usual one-body optical-model part. Since the true compound-nuclear states involve a complex sharing of energy among many nucleons, the transition to this complex situation must be via intermediate situations involving 2, 3, ... nucleons excited. If these intermediate "states" are *not* broad compared with their spacing, their structure will provide an additional modulation of the "strength functions" vs energy. Subthreshold nuclear fission has shown similar structure and yielded new insight into the physics of heavy nuclei.

The essential point which we emphasize is that one can never assume that existing simplified models have not, by definition, excluded important features of the actual interaction. It is essential to proceed with a systematic "filling in of the *experimental* picture" to see to what extent other important effects are present

The Columbia University Nevis synchrocyclotron has been used as a pulsed neutron source in an extended program of high-intensity high-resolution neutron time-of-flight spectroscopy. The emphasis in our previous papers[3] has been on intermediate- and heavy-weight nuclei which have high level densities and hence show large numbers of narrow resonances below 10-keV neutron energy. Our detailed analysis has tended to be limited to neutron energies below this energy using the single-level Breit-Wigner theory to analyze each resonance separately. The present paper is concerned with the analysis of part of the total-cross-section data obtained during 1962 and 1963 for elements showing strong wide resolvable resonance structure to several hundred keV energy. The preliminary analysis of the data for the natural elements Al, Ti, Fe, Ni, Cu, Zn, V, Mn, Co, and Bi was completed in 1964. Results[4] were presented in the form of curves of measured total cross section σ_T vs laboratory neutron energy E. Our experimental curves have been presented in great detail in the recent volumes of *Neutron Cross Sections*.[5]

The detailed level analyses for these elements has lagged, however, since our previous single-level analysis was considered to be inappropriate for these nuclei where resonance overlap is quite important. This paper presents the results of detailed analyses for the natural Ti, Fe, and Ni data using an R-matrix formalism. These elements all lie in the region of a maximum of the s-wave neutron strength function. The calculations were carried out at the State University of New York at Albany.

II. EXPERIMENTAL ARRANGEMENT AND PROCEDURE

A detailed description of the experimental system as used for these measurements has been given previously.[6] It should be referred to for more complete details. A brief description of the operation when these data were taken is presented below.

The synchrocyclotron accelerated protons in bunches (60 bunches per second for these measurements) to an energy of about 350 MeV. When the proton orbit radius was ~68 in. in the accelerator, a pulse ~100 kV was suddenly applied between deflection plates with respect to which the bunch was centered. This deflected the proton bunch downward onto a lead target. Several evaporation fast neutrons were produced per incident proton on the Pb target during a burst time $\leq$100 nsec. The instantaneous evaporation-neutron intensity during the burst was ~10^{18} to 10^{19}/sec (see Fig. 1 of A). A hydrogenous moderator (polyethelene) was situated just below the lead target so a pulse of moderated neutrons of all energies up to a few MeV was emitted in a pulse at $t=0$ from the front face of the moderator. The useful part of this flux was directed toward a 12-in.$\times$48-in.$\times 1\frac{1}{2}$-in. rectangular slab of B^{10} situated about 200 m from the source. The $B^{10}(n, \alpha)Li^{7*}$ reaction usually results in the emission of a 480-keV deexcitation γ ray which was detected by a bank of NaI detectors mounted either (a) in the collimated beam path directly behind the B^{10} slab, or (b) directly above the B^{10} slab out of the direct flight path.

The collimated flight path was mainly through helium-filled balloons to avoid the large scattering attenuation which would result for a path in air. Figure 2 of A[6] provides a plan view of the system. The neutrons first passed through a collimation aperture through the 10-ft-thick main cyclotron shield. A transmission sample station was located outside this shield so one could make "open-beam" or "sample-in" transmission measurements using various transmission sample elements and sample thickness for total-cross-section measurements. There was also optional provision to use a "fast chopper" or a "slow chopper" in the flight path to pass a group of neutrons and then block the flight path when the neutron bunch reached the detector station. The use of these choppers to reduce detector background due to γ rays from the target is described in A.[6] The detected neutrons were sorted according to their time of flight t by a 2000-channel analyzer system having 100-nsec timing channel widths. This

provided 0.5 nsec/m time-of-flight resolution in the region above 1-keV neutron energy. The implied energy resolution ΔE varied as $E^{3/2}$ and was about 10 eV at 10 keV, 50 eV at 25 keV, 150 eV at 50 keV, and 430 eV at 100 keV. At energies below about 100 keV this represented the highest experimental energy resolution of any neutron spectroscopy system. Above 100 keV the energy resolution was somewhat poorer than the best resolution achieved by other methods.[7]

The neutron detection pulses were sent to a 2000-channel time-of-flight analyzer system which is described in detail in A.[6]

III. BACKGROUND EVALUATION

Our previous papers have dealt with the neutron-energy region below ~10 keV, where background corrections can be made relatively easily. The present paper deals with energies $\lesssim$200 keV where the logic is more complicated as discussed below. The neutron detector consists of a large slab of B^{10} which is viewed by a bank of NaI scintillation γ-ray detectors which are also sensitive to various background radiation. This includes cosmic rays, natural γ radioactivity in the surrounding building materials, and long and short half-life radioactivity induced in the NaI crystals, and in the other materials in the neighborhood of the detector by previous neutron flux from the cyclotron. It also has a contribution from γ rays traversing the flight path from the cyclotron chamber.

The background counting rate is regarded as having a "constant" cyclotron independent term which is found by counting with the cyclotron off. In fact, however, this rate depends on the earlier cyclotron operation history because of the $\gtrsim$30-min half-life radioactivity induced at or near the detector, or inside the cyclotron and "viewed" from the detector via the flight path. The "constant portion" is subtracted from the count before determining the portion which is strongly energy and transmission sample dependent. Measurements with the cyclotron *off* gives a uniform counting rate in the 2000 channels corresponding to about 4% of the "open-beam" cyclotron-*on* intensity near 4 keV, and about 0.2% of the open-beam intensity near 200 keV.

The major contribution to the total background in the upper-keV region is from the delayed effects of higher-energy neutrons of the given burst which give delayed detector counts after scattering near the detector, plus γ rays from the cyclotron associated with the production of short-lived radioisotopes produced in the cyclotron with about 1- to 100-μsec half-life. The sample dependence of this high-energy region background is due to the attenuation by the sample of the faster neutrons, or of cyclotron γ rays which produce counts at the 200-m detector.

For measurements above a few keV the fast chopper,[6] situated immediately before the sample changer, was phased to be fully open at the time of the neutron burst and fully closed 50 μsec after the neutron burst. Since the chopper is made of tungsten (a high-Z element) it was very effective in stopping most of the γ rays when closed. Hence the background contribution from cyclotron γ rays was large for $t<50$ μsec and small for $t>50$ μsec. The maximum background was at $t=0$, when the chopper was fully open. Since the contribution of this background was a function of the γ-ray absorption coefficient of the transmission sample used, it was smaller when high-Z element transmission samples were used.

The background function after subtraction of the uniform background thus consisted mainly of two components:

(a) For $t>50$ μsec, it was mainly due to the scattered neutrons.

(b) For $t<50$ μsec, it had contributions from both sources mentioned above.

In our earlier measurements of the neutron cross sections, below about 10-keV neutron energy, the bank of NaI counters detecting the γ rays produced in the B^{10} was situated in the path of the neutron beam in order to obtain the maximum solid angle at the B^{10} detector. This arrangement had the disadvantage that the counters also saw the γ rays coming directly from the cyclotron area. The B^{10} detector was not completely opaque to the fast neutrons. Some of these neutrons were scattered from the counters and produced further events in the B^{10} slab at slightly later times. Moreover, some of these neutrons were captured by the iodine of the crystals and produced the radioactive isomer of iodine having a half-life of 30 min, thus contributing to the over-all background. For the measurements at higher neutron energy discussed here, the bank of NaI counters was placed above the B^{10} slab out of the line of the neutron flight path as shown in Fig. 3 of A.[6] The open-beam counting rates and the over-all background rates normalized to the same time (30 min) in these two separate runs was evaluated in the manner discussed below. These rates are shown in Figs. 1 and 2. These figures show that the background was reduced by a factor of 2 relative to the open-beam counts, although the solid angle and thus the over-all intensity was reduced by a factor of 3. Since our neutron intensity in this energy region was sufficiently high, this reduction in the intensity did not cause much inconvenience.

The background shown in Figs. 1 and 2 was care-

fully evaluated by examining the counts at the transmission dips of many strong resonances in many elements of varying thickness. The residual count rate at these minima, whenever the resonance was completely black (i.e., $n\sigma > 5$), was assumed to be the background count. In some cases two or more samples of the same element provided saturated dips for the same resonance and thus provided an estimate of the background dependence on the samples of varying thicknesses. Some of the elements and the resonance used in this evaluation are shown in Table I.

In this manner a direct dependence of the background counts vs total counts of each sample was established. This fact allowed us to determine the background function for the open beam. The maximum background was about 25% of the open-beam counts with the detectors in the beam behind the boron slab and about 12% of the open beam when the detectors were not in the beam. We feel that our evaluation of the background for open beam in both cases was better than 10% of the neutron intensity near the highest energy investigated and probably better than 5% of the open beam for energies below 100 keV.

Neutron transmission measurements were made in two different energy regions with different overall resolution:

(1) from 200 to 4000 eV,

(2) from 4 to 220 keV.

For the measurements in the low-energy region the time analyzer was set with a channel width of 0.4 μsec. The latter factor gave an energy resolution of 15 eV at 4000 eV, which is much smaller than the average spacing of levels for these elements, and hence was quite adequate to resolve all the levels in this energy region for all the nuclei investigated. Moreover, in many cases where the resonances were broad, the counts were averaged over many channels, sometimes as many as 27 channels, in order to obtain better statistical accuracy for the cross-section values.

The energy region above 4 keV was investigated using a channel width of 0.1 μsec. Since the energy resolution ($\Delta E/E$) was 0.1% at 4 keV and 1% at 300 keV, the ability to effectively resolve levels depends both upon the average energy-level spacing of the particular nucleus investigated and the

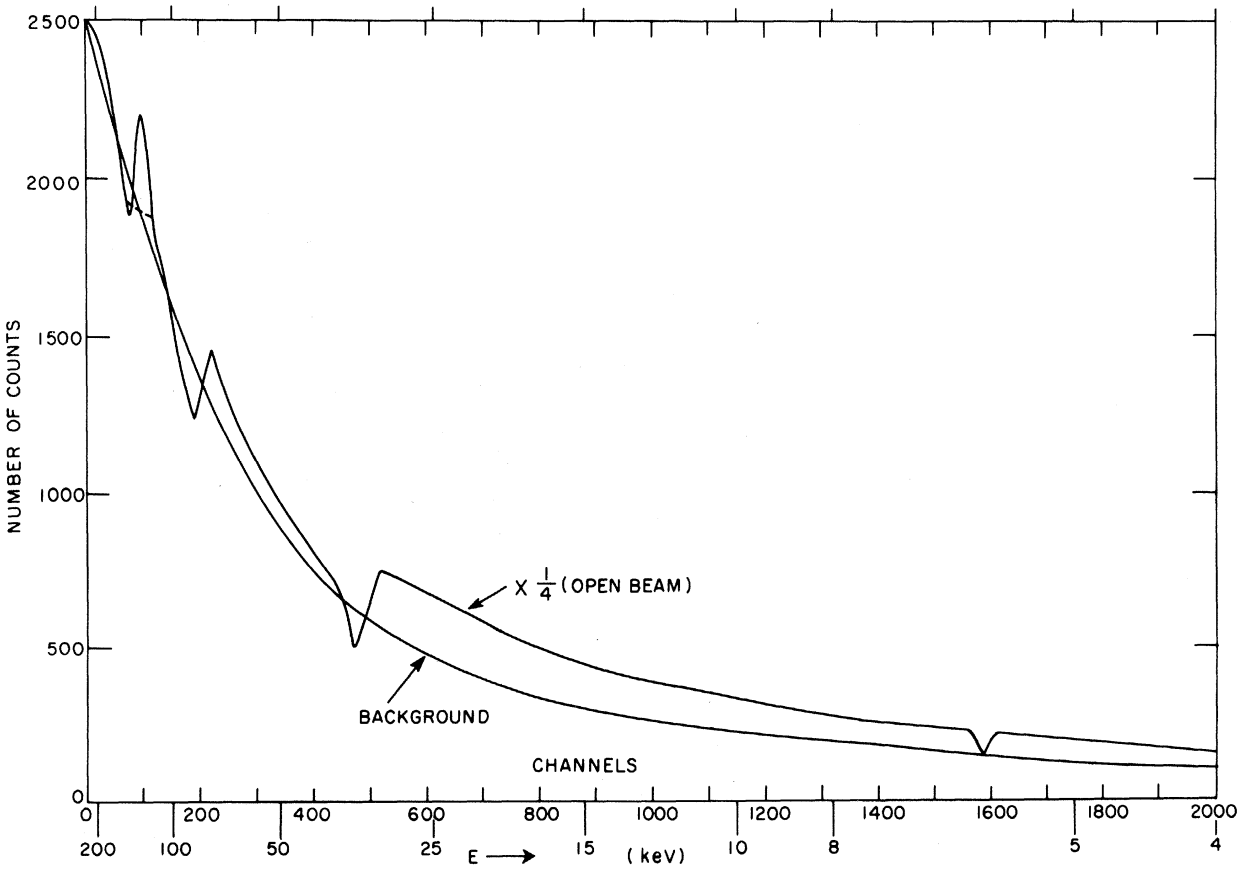

FIG. 1. The open-beam counts and the estimated total background counts are shown as a function of neutron energy. The neutron flight path is 200 m and the channel width is 0.1 μsec. The bank of NaI detectors was mounted facing the B^{10} slab in the line of the neutron beam.

maximum energy at which the data were taken. For most of the elements where the average spacing is of the order of 10 keV or greater, this resolution was adequate to resolve practically all levels up to 200 keV, or somewhat above this energy in some cases.

For most of the nuclei investigated, many samples of different thicknesses were used in order to obtain reliable values of the peak cross section as well as cross sections between peaks. The transmission measurements were made by alternately taking data with open beam and with the transmission sample in place. The raw data were processed using IBM type-1620 and -7090 computers at various stages. The output of each stage was carefully checked for consistency and other possible errors. The resulting detailed σ vs E curves have been given elsewhere.[4,5]

The other resonance parameters which are of interest in addition to the level energies are the spins and the neutron widths of the levels. It is also desirable to know the isotopic assignment of each particular level where a natural element is used for the measurements.

IV. RESONANCE ANALYSIS THEORY

The natural elements treated in this paper have the following atom percent isotopic composition. Natural Ti has 7.99% Ti^{46} ($I=0$), 7.32% Ti^{47} ($I=\frac{5}{2}$), 73.99% Ti^{48} ($I=0$), 5.46% Ti^{49} ($I=\frac{7}{2}$), and 5.25% Ti^{50} ($I=0$). Natural Fe has 5.84% Fe^{54} ($I=0$), 91.68% Fe^{56} ($I=0$), 2.17% Fe^{57} ($I=\frac{1}{2}$), and 0.31% Fe^{58} ($I=0$). Natural Ni has 67.76% Ni^{58} ($I=0$), 26.16% Ni^{60} ($I=0$), 1.25% Ni^{61} ($I=\frac{3}{2}$), 3.66% Ni^{62} ($I=0$), and 1.16% Ni^{64} ($I=0$).

The observed cross section for each natural element is the sum of the separate contributions from the component isotopes. For an even-even $I=0$ target nucleus we can only have a single $J=\frac{1}{2}^+$ compound-nucleus state for $l=0$ neutrons, but we can have $J=\frac{1}{2}$ or $\frac{3}{2}$ opposite-parity states for $l=1$ neutrons. These three states give independent contributions to the total cross section. For odd-A nuclei, $I\neq 0$, so $J=I-\frac{1}{2}$ or $I+\frac{1}{2}$ for $l=0$ neutrons, with relative spin statistical weighting $g_J=I/(2I+1)$ for $(I-\frac{1}{2})$ and $(I+1)/(2I+1)$ for $(I+\frac{1}{2})$. These two compound-nuclear spin populations contribute independently to the total cross section. For $l=1$

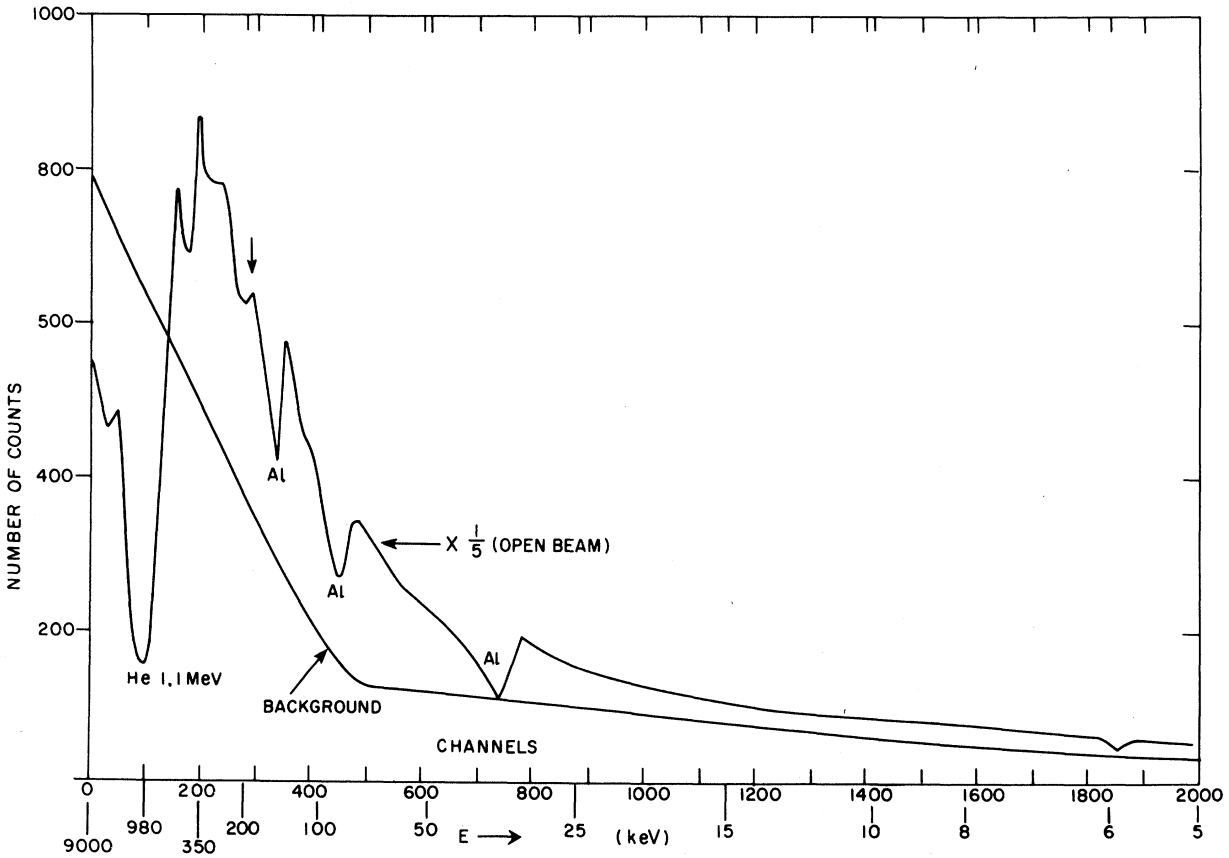

FIG. 2. The open-beam counts and the estimated total background counts are shown as a function of neutron energy. The bank of NaI detectors was mounted above the B^{10} slab out of the neutron beam.

neutrons $J = I - \frac{3}{2}$, $I - \frac{1}{2}$, $I + \frac{1}{2}$, and $I + \frac{3}{2}$ with spin weighting $g_J = (2J+1)/2(2I+1)$. These compound-nuclear states again each give independent contributions to the total cross section.

For a neutron of incident kinetic energy E in the laboratory frame, the momentum p of the *relative* motion is $[A/(A+1)](2mE)^{1/2}$, where m is the neutron mass. Near resonances the cross section tends to be expressed in units of $\lambda\!\!\!^{-2} = \hbar^2/p^2$. For low-$A$ nuclei it is important to note that $\lambda\!\!\!^{-2}$ is $[(A+1)/A]^2$ times larger than one would calculate for an infinite target mass. Resonance energies and partial resonance level widths are usually expressed in units of the laboratory neutron kinetic energy rather than the relative motion energy. Since these energies usually appear as dimensionless ratios in the resonance cross-section expression, one must use the same convention for all the quantities. We have chosen to express our results in laboratory energy units.

For $l=0$ neutrons interacting with the nucleus to form a state of definite J, the neutron radial wave function has the form

$$\Phi = r\psi \sim (e^{-ikr} - U_J e^{ikr}), \tag{1}$$

and various cross sections are given as

$$\sigma_{\text{scatt}} = \pi\lambda\!\!\!^{-2} \sum g_J |1 - U_J|^2, \tag{2a}$$

$$\sigma_{\text{abs}} = \pi\lambda\!\!\!^{-2} \sum g_J (1 - |U_J|^2), \tag{2b}$$

$$\sigma_{\text{tot}} = 2\pi\lambda\!\!\!^{-2} \sum g_J (1 - \text{Re}U_J). \tag{2c}$$

The collision function U_J is a complex number in this case with $|U_J| \leq 1$, and $|U_J| = 1$ if only scattering is present. In the present situation for Ti, Fe, and Ni, the scattering dominates over capture almost everywhere. If we neglect capture we see that $(\sigma/\pi g_J \lambda\!\!\!^{-2})$ varies between 0 and 4 for the particular compound-nucleus contribution. The peak (natural-element) value $\sigma = 4\pi f g_J \lambda\!\!\!^{-2}$ occurs near the resonance energy. The magnitude of the peak, aside from known energy factors, is proportional to fg_J, so one can usually establish the responsible isotopes (of fractional abundance f) *and* the J value of the resonance. In cases where the identification is previously known, or is unambiguous, it also provides a test on the accuracy of the peak cross-section measurement if contributions from other isotopes and spin states are small. If two overlapping resonances do not show a strong (interference) minimum it usually means that either they belong to different compound nuclei, or have different J or parity. For adjacent scattering resonances of the same compound nucleus and J, the value of U_J passes near unity between levels, and there is a (near) zero contribution from the reso-

TABLE I. Elements having bottoming resonance transmission dips ($T=0$) used for background evaluation. The approximate energies and the corresponding cross sections are indicated.

Element	Approximate resonance energies (keV)	Approximately measured σ_t (b)	Element	Approximate resonance energies (keV)	Approximately measured σ_t (b)
Al	35	34	Co	4	350
	88	18		5	235
	150	14		8	120
				10	120
Ti	17	115		17	90
	22	90		25	60
	37	55		35	43
	52	38		51	23
V	4	365	Cu	5	200
	7	180		8	90
	22	55		13	85
	40	30		18	65
Fe	28	88	Zn	11	130
	84	30		13	100
	140	17		19	45
	188	13		24	35
Mn	7	200		32	35
	35	45	Bi	5	250
	58			12	100
Ni	15	110		16	80
	64	30		33	40
	140	13			

nant channel between the resonances. This often provides a test as to whether or not adjacent wide resonances are for the same compound nucleus having same J^{π}.

In both the Feshbach, Peaslee, and Weisskopf (F.P.W.) theory[8] and the Wigner-Eisenbud R-matrix theory,[9] attention is focused on the behavior of the radial wave at the "neutron channel radius" $r=R$. This radius is essentially equal to the radius where the neutron-nucleus interaction first becomes significant. The F.P.W. theory considers the energy dependence of the logarithmic derivative of the neutron channel radial wave function at $r=R$:

$$F=\frac{r}{\phi}\frac{d\phi}{dr}, \quad r=R. \tag{3}$$

Between resonances F is large because the extrapolated radial function ϕ tends to have a node near $r=R$ (potential scattering). If $kR \ll 1$, a resonance occurs when $F=0$. The neutron width of the resonance is inversely proportional to dF/dE in the region where $F=0$.

The R-matrix formalism derives an explicit form for the variation of F with E in terms of the resonance parameters. A very detailed review of

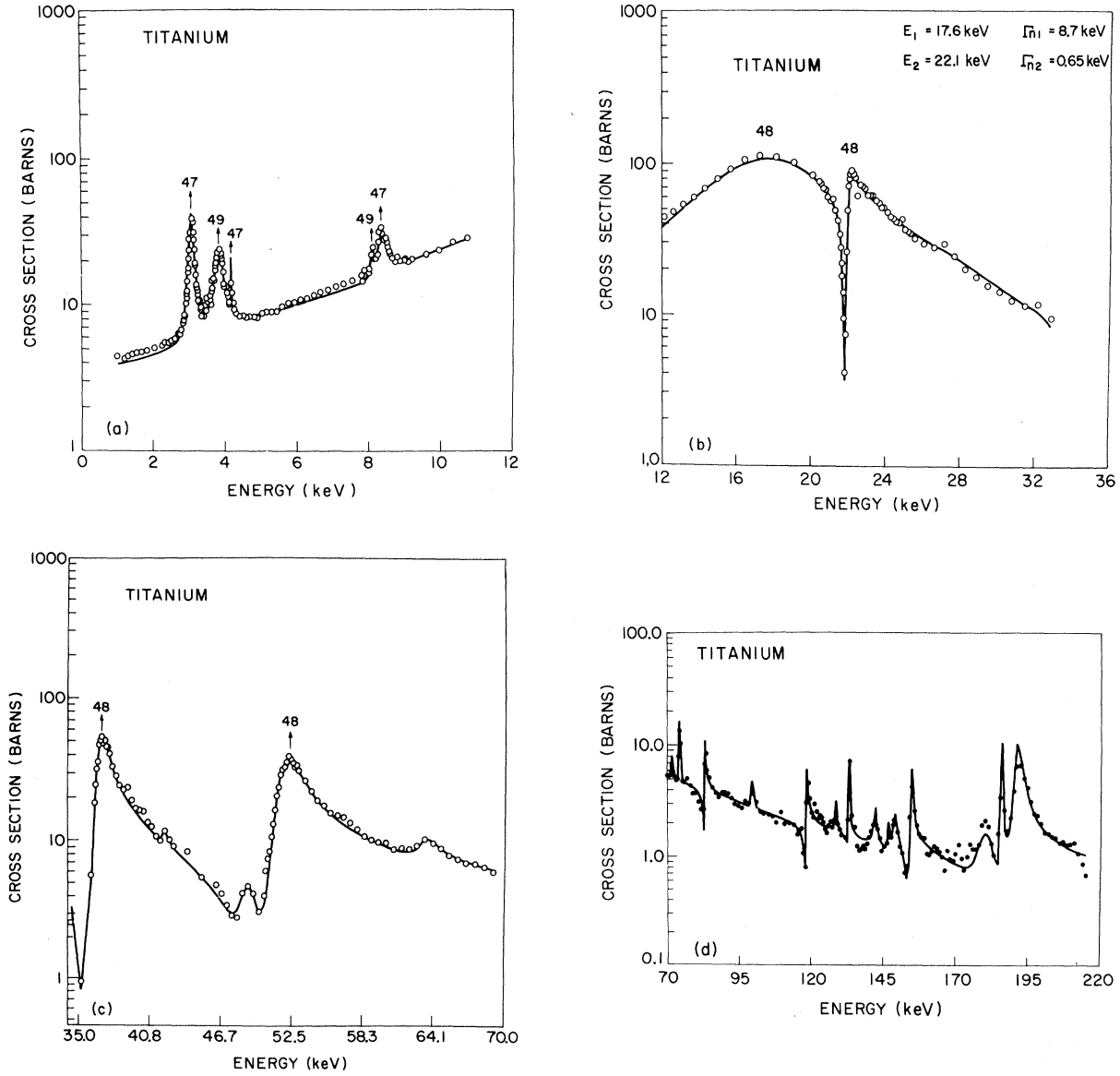

FIG. 3. (a)–(d) The observed neutron total cross section of titanium in the energy region up to 215 keV. The data have been averaged over many channels in between the resonances. The smooth curve is the R-matrix fit with the resonance parameters as given in Table II.

this theory has been given by Lane and Thomas[10] (L.T.). In this paper we have followed the procedures used by Firk, Lynn, and Moxon[11] (F.L.M.) for the analysis of the total neutron cross-section results for V^{51}. The full R-matrix theory requires a complicated matrix inversion when many channels are important. The simplification used here is possible in the case where channels other than elastic scattering give only a small correction to the expression derived assuming that only the incident channel contributes. One then has the U matrix for $l=0$ neutrons

$$U_J = e^{-2ika}\frac{1-ikaR_J}{i+ikaR_J}, \tag{4}$$

where

$$R_J = \sum_{\lambda J}\frac{\gamma_{\lambda J}{}^2}{E_{\lambda J}-E-\frac{1}{2}i\Gamma_{\lambda J r}}. \tag{5}$$

The $E_{\lambda J}$ are the resonance energies. The parameter λ indicates which resonance, and J indicates the angular momentum of the compound nucleus. The $\Gamma_{\lambda J r}$ represents the capture width for the level treated in a manner similar to that of F.P.W. (i.e., the resonance energies $E=E_{\lambda J}-\frac{1}{2}i\Gamma_{\lambda J r}$ correspond to a time decay of the eigenstate via the capture channel), where the decay rate is proportional to $\Gamma_{\lambda J r}$.

In the more general R-matrix theory (Ref. 10, p. 276), the resonance energy is taken as $E_\lambda+\Delta_\lambda$, where Δ_λ is a level-shift parameter. The resonance energies are the "energies at which the resonance contribution to the phase-shift formula is equal to odd integral multiplies of $\frac{1}{2}\pi$." For $l=0$ neutrons $\Delta_\lambda=0$. We define our resonance energies in this paper to be just the $E_{\lambda J}$ values in Eq. (5), for s-wave levels. For the few weak p-wave levels, E_λ was given as the actual observed level energy.

The expression for R_J should be summed over all energies. Following F.L.M.[11] we divide the

TABLE II. Parameters of resonances observed in natural titanium as determined by the R-matrix analysis of the neutron total cross section. The energies are in the laboratory system.

	E_0 (keV)	Γ_n (keV)	Γ_n^0 (eV)	J^π	S_0 (units of 10^{-4})
Ti^{48}	17.6 ±0.1	8.71 ±0.10	65.66±1.31	$\frac{1}{2}^+$	
	22.1 ±0.1	0.65 ±0.05	4.37±0.34	$\frac{1}{2}^+$	
	36.8 ±0.1	1.25 ±0.10	6.52±0.52	$\frac{1}{2}^+$	
	51.9 ±0.2	2.36 ±0.20	10.36±0.88	$\frac{1}{2}^+$	
	74.2 ±0.2	0.15 ±0.10	0.55±0.37	···	4.92±2.18
	83.2 ±0.4	0.13 ±0.10	0.45±0.35	$\frac{1}{2}^+$	
	118.6 ±0.6	0.20	0.58	$\frac{1}{2}^+$	
	133.0 ±0.8	0.16	0.44	···	
	154.5 ±0.9	0.43	1.09	$\frac{1}{2}^+$	
	185 ±1	0.76	1.77	···	
	191 ±1	2.89	6.61	$\frac{1}{2}^+$	
Ti^{49}	3.835±0.005	0.259 ±0.013	4.19±0.21		
	8.095±0.01	0.08 ±0.01	0.88±0.11		2.64±1.90
	27.30 ±0.05	0.36 ±0.04	2.18±0.24		
	32.30 ±0.10	0.36 ±0.04	2.00±0.22		
Ti^{50}	90.10 ±0.50	0.99	3.29	$\frac{1}{2}^+$	
	146.8 ±1	0.42	1.10	$\frac{1}{2}^+$	
	185.6 ±1	1.52	3.53	$\frac{1}{2}^+$	
Ti^{46}	48.9 ±0.2	1.75	7.91	$\frac{1}{2}^+$	
	63.5 ±0.2	1.66	6.59	$\frac{1}{2}^+$	
	71.6 ±0.3	0.12	0.45	$\frac{1}{2}^+$	
	99.8 ±0.4	0.07	0.22	$\frac{1}{2}^+$	2.34±1.20
	128.5 ±0.6	0.55	1.53	$\frac{1}{2}^+$	
	142.0 ±0.8	1.33	3.53	$\frac{1}{2}^+$	
	148.8 ±0.8	1.70	4.41	$\frac{1}{2}^+$	
	171.0 ±0.9	0.90	2.18	$\frac{1}{2}^+$	
	179.4 ±1.0	6.53	15.42	$\frac{1}{2}^+$	
Ti^{47}	3.074±0.004	0.134 ±0.006	2.42±0.11	3^-	
	4.180±0.004	0.0028±0.0014	0.04±0.02	3^-	1.63±1.40
	8.350±0.01	0.28 ±0.02	3.06±0.22	3^-	
	42.1 ±0.2	0.27 ±0.05	1.32±0.24	3^-	

contribution into those from the studied energy region where resonance effects are specifically included in the sum, and contributions from negative and positive energies outside this energy range

$$R_J = R_J(\text{local}) + R_J(\text{residual}). \tag{6}$$

The analytic form of R_J(residual) has no poles in the fitted region and can be expanded in a Taylor series expansion in powers of $(E - E_{1/2})$, where $E_{1/2}$ is the center of the energy region analyzed. The slope of R_J(residual) must always be positive. Following F.L.M.[11] we use only the constant and linear terms in the expansion:

$$R_J(\text{residual}) = A_J + B_J(E - E_{1/2}). \tag{7}$$

The portion A_J contains the effect of the potential scattering amplitude, including optical-model effects. F.L.M. show that the value of B_J provides an independent evaluation of the s-wave strength function for the given compound nucleus and J for the energy regions above and below that treated in the main analysis.

The resonance-neutron channel partial width is related to the $\gamma_{n\lambda J}{}^2$ as

$$\Gamma^0_{n\lambda J} = 2ka\gamma_{n\lambda J}{}^2(l=0). \tag{8}$$

The reduced neutron partial width is sometimes defined as $\gamma_{\lambda J}{}^2$, but we have favored the form

$$\Gamma^0_{n\lambda J} = \Gamma_{n\lambda J}[(1\text{ eV})/E]^{1/2},\ (l=0). \tag{9}$$

If $\langle D_J\rangle$ is the mean s-wave level spacing for the given compound nucleus and J, the strength function S_{0J} is either defined as

$$S_0 = \langle\gamma_{\lambda J}{}^2\rangle/\langle D\rangle_J \tag{10a}$$

or as

$$S_0 = \langle\Gamma^0_{n\lambda J}\rangle/\langle D\rangle_J \tag{10b}$$

using Eq. (9). We favor the use of form (10b).

When fitting the measured $\sigma(E)$ for natural Ti, Fe, or Ni, we note that the observed $\sigma(E)$ is the sum, weighted in proportion to the isotopic abundances and spin factors, of the various sample isotopic components, and the various compound nucleus J states. For *each* such contribution we must, in principle, adopt a set of A_J, B_J, $\Gamma_{n\lambda J}$, and $E_{\lambda J}$ values. In addition to the energy region which we study, one often has information available on the thermal-neutron-capture cross section and the thermal coherent and incoherent scattering cross sections. In making a detailed fit to the total experimental information it is sometimes necessary to include a negative-energy resonance for one of the isotopes and J values. The $\Gamma_{n\lambda J}$ and $|E_\lambda|$ for this resonance are then parameters to be chosen for a best over-all fit. The negative-energy resonance mainly affects the cross section near zero neutron energy.

In general, in the first few attempts one can obtain reasonable values of these parameters. From there on the final fit is obtained by varying these quantities by observation of the agreement of the computed and measured cross-section values. It is usually the thermal-capture cross section which determines the value of Γ_γ for the most prominent resonances or the presence of a negative bound level and its resonance parameters. The value of the radius is determined by using the relation $R = r_0 A^{1/3}$, and we have rounded it off to the nearest half-integral value. The resonance parameters obtained are usually not sensitive to small variation in this value of R; however, this choice does affect the value of the cross section between resonances and in the thermal region.

The present program uses the same value of R for all the isotopes and spin states. A modification for varying this parameter will be made in the future.

V. RESULTS

A. Titanium

Samples of natural-titanium metal sheets with $n^{-1} = 5.14$, 25.3, and 131 b/atom were used for the measurements over the whole energy region. The detailed cross-section-vs-energy curves and a list of preliminary values of resonance energies determined from the positions of the cross-section maxima have been reported elsewhere.[4,5] The total cross section of natural titanium has also been previously measured by Bilpuch *et al.*,[12] and resonances have been assigned to different isotopes. However, our results show a much more complicated resonance structure than that observed by Bilpuch *et al.*[12] In particular there are many narrow levels superposed on broad levels at 17, 37, and 52 keV. This is not surprising, since natural titanium has 5 isotopes of masses 46, 47, 48, 49, and 50 with varying abundances as mentioned earlier, and our resolution is very good at these energies. Assuming that all the observed resonances are due to s-wave interaction, each of the even-mass isotopes will form one type of spin states ($\frac{1}{2}^+$) but each odd-mass isotope would give rise to two different spin states ($I \pm \frac{1}{2}$). Hence one should observe resonances of at least seven independent spin states which add incoherently to give the total cross-section variation with energy for the natural element. Our analysis indicates that some resonances are also most likely p wave as evident from the lack of interference effects and from the σ values at the resonance peak. Resonances belonging to the same spin

states in the same isotope will give rise to coherent interference effects.

In the program used in this analysis, we can take into account the effects of only four different types of states at a time. For the isotopes considered these contribute to $\sum fg = 0.88$. Hence the calculated cross sections at any given energy would be smaller by $(0.12 \times \sigma_p)$ b than the actual cross sections if all seven states were included in the analysis. It is likely that σ_p for different isotopes may be different; however, in this analysis the same value of σ_p has been assumed for all the isotopes and spin states. σ_p is the average potential scattering cross section. Assuming a value of $\sigma_p = 3.14$ b the matching calculated σ_T values are made to be 0.38 b lower than they should be if the contributions from missing isotopes were added. However, for the final fitting in each energy region the appropriate contribution from low-abundance isotopes are taken into account.

The results of this analysis are shown by the solid curves in Fig. 3(a)–3(d). One notices that up to 70 keV there are 4 strong resonances whose peak cross sections correspond to the theoretically predicted cross sections for the most abundant isotope of mass 48. The strong interference minima near 22, 35, and 48 keV also indicate that these resonances belong to the same isotope and spin state. The data shown in these figures have been averaged over many channels for clarity and to reduce statistical fluctuations. [See Ref. 5 for a more-detailed plot of the data.] The narrowest resonance at 4.18 keV is significantly broader than our instrumental resolution and, on account of its low observed σ_T, it cannot be assigned to Ti^{48}, as has been done by Bilpuch *et al.*[12] The single level at 9 keV reported by Bilpuch *et al.*[12] also does not belong to Ti^{48}, and in our measurement it is observed as a doublet. These resonances must belong to isotopes of 47 and 49 on the basis of the observed peak cross sections. This assignment agrees with the results of Good *et al.*[13] obtained using separated isotopes of Ti^{47} and Ti^{49}.

For the evaluated resonance parameters it is possible to calculate the values of coherent scattering, capture, and scattering cross sections at thermal energies. These values[5] have been measured by various authors, and one can compare them with the calculated values obtained from our measurements of resonance parameters. The coherent scattering cross section $4\pi a^2$, is proportional to the scattering length a which can be either + or −. We list $(\sigma_{coh})^{1/2}$ with the *sign* of the scattering length, i.e., $(4\pi)^{1/2}a$.

Our best fit gives $(\sigma_{coh})^{1/2} = -1.30 \times 10^{-12}$ cm. This agrees with the recommended value[5] of $(-1.31 \pm 0.3) \times 10^{-12}$ cm for natural titanium. Including all isotopes we obtain $\sigma_s = 3.68 \pm 0.4$ b at zero energy, which agrees well with the directly measured value of 4 ± 1 b. The negative scattering length at $E = 0$ is due to the larger contribution of resonance scattering amplitude from the 17.6-keV level in Ti^{48} than the potential scattering amplitude with opposite sign.

The element titanium is one of the few elements possessing an anomalous negative scattering amplitude for slow neutrons. Shull, Wilkinson, and Mueller[14] have established that the most-abundant isotope of Ti^{48} is responsible for the anomalous scattering length with a value of -0.58×10^{-12} cm. This seems to be consistent with the broad resonance at 17.6 keV which produces destructive interference with the potential scattering near thermal energies.

In order to reproduce the measured value[5] of 6.1 b for the thermal capture cross section using only positive-energy resonances, it is necessary to assign a value of $\Gamma_\gamma = 8.2$ eV to the 17.6-keV resonance. For an equal value of Γ_γ, the other observed resonances in all isotopes give only a small contribution to thermal capture. For example, the 22-keV level contributes only ~0.3 b. Since a Γ_γ of 8.2 eV is larger than expected from the measured values for adjacent nuclei, one might try to account for the thermal σ_c as mainly due to the contribution from a negative (near-zero) energy level. However, unless unreasonable ratios of Γ_γ to Γ_n^0 are chosen for that level, the constraint of fitting σ_{coh} and σ scattering rules out such a bound level contribution. No direct measurement of the capture width for these resonances has been reported.

The large value of Γ_γ for Ti^{48} might be associat-

TABLE III. Values of the channel radii and the coefficients A_J and B_J used in the R-matrix analysis of the data.

		A_J	B_J
Channel radius $R = 6 \times 10^{-13}$ cm.			
Iron	Fe^{56}	0.09	0.03×10^{-4}
	Fe^{54}	0.04	0.2×10^{-4}
	Fe^{57}	0.1	0.01×10^{-4}
Channel radius $R = 5 \times 10^{-13}$ cm.			
Titanium	Ti^{48}	0.24	0.02×10^{-4}
	Ti^{47}	0.1	0.1×10^{-4}
	Ti^{49}	0.1	0.01×10^{-4}
	Ti^{46}	0.4	0.03×10^{-4}
Channel radius $R = 6 \times 10^{-13}$ cm.			
Nickel	Ni^{58}	0.29	0.12×10^{-4}
	Ni^{60}	−0.26	0.01×10^{-4}
	Ni^{62}	−0.13	0.1×10^{-8}
	Ni^{64}	0.1	0.1×10^{-4}

ed with the fact that the compound nucleus Ti^{49} has only one neutron less than the subshell value 28, so single-particle matrix elements may be particularly strong.

If one accepts the measured value of coherent scattering cross section at thermal energies, one gets a unique value of $\Gamma_n = 8710$ eV for the 17.6-keV resonance, with an uncertainty of about ±100 eV. This demonstrates the usefulness of the thermal data in determining the unique values of the parameters for the resonance mainly responsible for thermal cross sections.

The data at low energies from 2 to 10 keV were fitted to extract the parameters of resonances in other isotopes of titanium where the resonances are broader than our resolution. These results are also shown in Table II.

In addition to the resonances listed in Table II, many strong resonances have been observed at energies of 250±2, 271±3, 314±3, 368±4, 390 ±5, 404±6, 422±7, 458±8, 494±9, and 529±9 keV. These are due to the most abundant isotopes of Ti^{48}. The theoretical analysis to extract their widths is not very successful owing to the poorer resolution at these energies.

In addition there are many weak levels observed at 10.504±0.015, 11.055±0.030, 11.45±0.05, 12.13±0.05, 12.80±0.03, 13.45±0.03, 16.34±0.05, 23.8±0.05, 39.05±0.11, 43.8±0.1, 46.06±0.10, and 56.1±0.10 keV. Some of these levels have been also observed in the measurements of Good *et al.*[13] Since their resolution was poorer, they analyzed their data by area analysis to determine the neutron widths. Our resonance energies are systematically higher than their results.

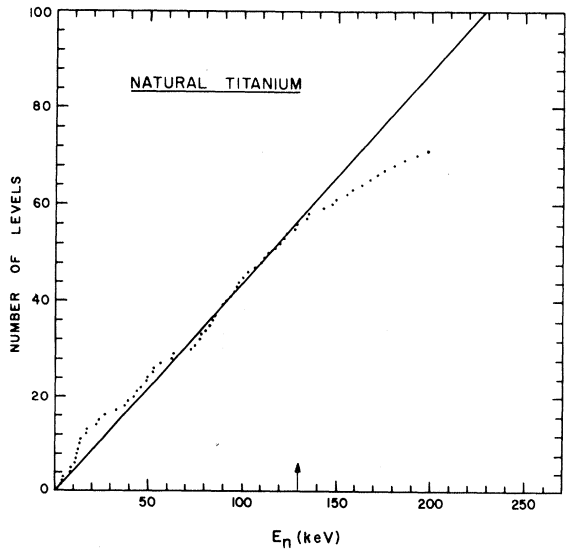

FIG. 4. A linear plot of the total number of resonances observed up to the energy E_n in the natural titanium. The slope of the straight line gives the average level spacing for the natural element.

The resonances in the energy range from 70 to 200 keV are relatively quite narrow and the structure is quite complex. However by using a similar analysis for that energy region, we are able to make the isotopic and l-value assignments of resonances in some cases. The lack of a minimum on the low-energy side and of interference between resonances seems to indicate that the resonances at 74.4, 133, and 185.6 keV are most likely strong p-wave resonances in Ti^{48}. However, since there is some uncertainty about the nature of these levels, these are treated as s-wave levels in the calculation of the s-wave level spacing and strength function. The analysis of these levels was performed by essentially using a single-level Breit-Wigner formalism with the value of σ_p assumed to be zero. Thus the stated level energies and Γ_n values are the actual energy position of the resonances and their observed widths.

Many of the resonances between 120~154 keV are most likely due to the isotopes Ti^{46} and Ti^{50}, since they are broad enough and the peak cross sections agree well with that expected theoretically for these isotopes. Since the odd isotopes usually have small level spacings, their resonances in general will have smaller widths and hence will not be resolved at higher energies.

The values of channel radii and the coefficients A_J and B_J used in our analysis for the titanium isotopes are given in Table III. The cross sections for separated isotopes of titanium has been more recently measured by the Duke group[7] with much better resolution than their earlier measurements[12] in the energy range of 3–80 keV. The cross section for Ti^{46} and Ti^{50} were corrected for oxygen and the presence of Ti^{48}. The Ti^{48} sample was used enriched to 99.5% in the form of metal. For these measurements they have used shape analysis. Our resonance energies are in excellent agreement with theirs, although there is some disagreement in the measured values of the neutron widths.

Mean Level Spacings and Strength Function

For the particular case of Ti^{48} there seem to be 11 $l=0$ levels up to 200 keV, which give a value for the mean $l=0$ spacing $\langle D\rangle = 18\pm3$ keV. The corresponding s-wave mean level spacing for Ti^{46} is 22±3 keV. The data for other isotopes of titanium are too incomplete to determine the mean spacings, since many observed weak levels have not been identified. The neutron width of the level at 17.3 keV is unusually large. This width is 8.7 keV, which is about $\frac{1}{2}$ of the mean spacing D. Similarly the observed width of the levels at 22, 37,

and 52 keV are about 0.65, 1.25, and 2.3 keV, respectively. Thus most of the strength function is contributed by the first four resonances. This may represent an intermediate-structure effect. A linear plot of all the levels observed in natural titanium vs neutron energy is shown in Fig. 4. If the assumption of constant level spacing is true, very few $l=0$ levels are missed up to 130-keV neutron energy, above which the observed level density seems to decrease. Probably some levels are being missed because of our diminishing instrumental resolution. The $l=0$ strength function for Ti^{48} is $S_0=(15.8\pm11.5)\times10^{-4}$ for the region to 50 keV, but only $(4.92\pm2.18)\times10^{-4}$ for the full region to 200 keV.

The $l=0$ strength function for Ti^{46} is $(2.34\pm1.20)\times10^{-4}$ and for Ti^{47} is $(5.55\pm4.65)\times10^{-4}$ up to 10 keV but smaller if computed up to higher energies. For Ti^{49} up to 35 keV it is $(2.64\pm1.85)\times10^{-4}$.

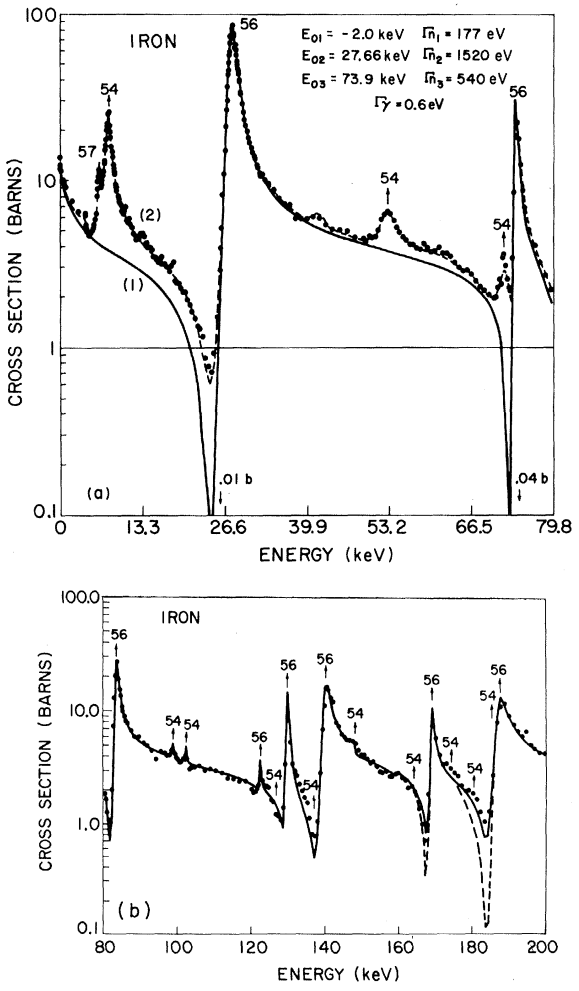

FIG. 5. (a), (b) The observed neutron total cross section in natural iron in the energy region up to 200 keV. The data have been averaged over many channels in between the resonance structure and on the resonance peaks when the peaks are much broader than the instrumental resolution. The curves are the R-matrix fit with the resonance parameters as given in the Table IV.

B. Iron

Samples of Armco sheet iron with $n^{-1}=1.16$, 4.65, 18.61, and 74.46 b/atom were used for the measurements. The total cross sections for natural iron and for the separated isotopes Fe^{54} and Fe^{56} have also been measured by Hibdon[15] and more recently by Newson *et al.*[16] Our results are essentially in agreement with their data, except in a few cases. Since natural iron has three main isotopes with masses of 54, 56, and 57, of varying abundances as indicated earlier, and <1% Fe^{58}; the most abundant Fe^{56} dominated the cross sections. It was rather difficult to see levels due to the less-abundant isotopes of mass 54 and 57 whenever they are superposed on a strong level of the most abundant isotope of mass 56.

The initial analysis of the data up to 80 keV for an R-matrix fit only considered the Fe^{56} contribution. The levels at 27.66 and 73.9 keV show strong interference minima and are thus $l=0$ levels. Also there is a minimum on the low-energy side of the 27.66-keV level and a rising cross section with decreasing energy near zero energy. In our analysis we also use the thermal-neutron scattering cross sections.[5] To match the rising cross section near $E=0$ we insert a bound s-wave level at an *a priori* unknown energy with a value for Γ_n. A value of $\Gamma_\gamma=0.6$ eV was used for all of the levels to agree with the measured[17] value of Γ_γ for the 1167 eV $l=1$ capture level in Fe^{56}. For the best-fit choice of parameters of Fe^{56} a comparison of the data with the theoretical best-fitting curve is shown in Fig. 5(a) as the smooth curve labeled (1). Since the theoretical curve does not include contributions from the other isotopes, it fits where σ_T is large and is below the experimental values at lower E_n by an amount indicative of the contribution of the other isotopes. The nonzero Fe^{56} cross section at the interference minima is due to the contribution from neutron capture. The $l=0$ parameters for Fe^{56} in Fig. 5(a) were actually the result of an iterative search for a "best match" also including fits to the contributions from the other isotopes.

The broken curve labeled (2) in Fig. 5(a) shows the fit obtained including contributions from the other isotopes of masses 54 and 57. The isotope choice for each residual structure after subtracting the Fe^{56} contribution was based on the implied abundance times statistical weight factor to give the observed resonance peak heights. The resulting isotopic identifications are marked on the figures.

Using these resonance parameters as indicated in Table IV, we obtain $(\sigma_{coh})^{1/2} = +3.25 \times 10^{-12}$ cm, compared with the measured value[5] of $+3.26 \times 10^{-12}$ cm, in excellent agreement. Note that one does not *just* choose the negative-energy resonance parameters to fit σ_{coh}, because the curve must also fit the low-energy end of *our* data.

The thermal-capture cross section is mainly due to contribution from the bound state. The value $\sigma_{cap} = 2.55 \pm 0.5$ b and $\sigma_s = 11 \pm 1$ for natural iron have been previously measured.[5]

There is really no "left-over" degree of freedom in choosing E_0 and the negative-energy resonance to fit the low-energy end of our cross-section plus the thermal-scattering data. This is easily seen as follows: the amplitude contribution to the scattering from the negative-energy resonance is proportional to $\Gamma_n^0/(E - E_0)$. For a given E_0, one can always choose Γ_n^0 to fit the thermal data. However, the rate of drop-off is then very dependent on the value of E_0 chosen. The match for the region $E = 0$ to 5 keV is then quite dependent on the choice of E_0 for the bound level, and a unique selection is required to fit this part of the data. Our value $E_0 = -2.0$ keV disagrees with Moore's[17] value of $E_0 = -4.39$ keV. Our result is from a complete fitting of a more complete set of data. Our E_0, Γ_n^0 choices then require a value $\Gamma_\gamma = 0.64$ eV to fit the measured thermal-capture cross section. Moore would necessarily need a different choice of Γ_γ for his different Γ_n^0, E_0 to match the thermal data.

The data from 80 to 200 keV, Fig. 5(b), were analyzed in a similar way. The large resonances showing well-defined interference minima in the cross section are clearly s-wave levels in Fe^{56}. The level at 122.5 keV is also s wave since definite interference structure is present and the results of Bowman, Bilpuch, and Newson[18] using separated iron isotopes confirm that the resonance is in Fe^{56}. Fe^{54} is responsible for most of the remaining predominant structure. The separated isotopes measurement results of Bowman, Bilpuch, and Newson[18] were used as a guide to note situations where Fe^{54} resonances occur at essentially the same energy as prominent Fe^{56} levels. However, our final fit involved independent searching for the best Fe^{54} parameters and is not simply using the parameters of Bowman, Bilpuch, and Newson.[18] The resonance parameters for the final theoretical fit are given in Table IV. In addition to the resonances listed in Table IV many weak resonances at energies 4.714 ± 0.004, 5.543 ± 0.006, 9.476 ± 0.013, 10.342 ± 0.015, 11.169 ± 0.016, 13.973 ± 0.020, 39.36 ± 0.10, 42.07 ± 0.10, 46.0 ± 0.1, 76.9 ± 0.3, 80.6 ± 0.4, and 90.2 ± 0.5 keV have also been observed. On account of their weak character neither a determination of their widths nor isotopic assignments can be made. However, these are most likely p-wave resonances.

The value of mean level spacing for Fe^{54} and Fe^{56} is 20 ± 3.5 and 25 ± 4 keV, respectively. It

TABLE IV. Parameters of resonances observed in natural iron as determined by the R-matrix analysis of the neutron total cross section. The energies are given in the laboratory system.

	E_0 (keV)	Γ_n (keV)	Γ_n^0 (eV)	J^π	S_0 (units of 10^{-4})
Fe^{54}	7.757 ± 0.010	1.02 ± 0.02	11.58 ± 0.23	$\frac{1}{2}^+$	
	52.5 ± 0.2	2.54 ± 0.12	11.10 ± 0.52	$\frac{1}{2}^+$	
	71.8 ± 0.3	2.48 ± 0.21	9.26 ± 0.78	$\frac{1}{2}^+$	
	98.5 ± 0.4	0.58 ± 0.16	1.85 ± 0.51	$\frac{1}{2}^+$	
	102.0 ± 0.5	0.59 ± 0.25	1.85 ± 0.78	$\frac{1}{2}^+$	3.2 ± 1.6
	128.5 ± 0.6	0.95 ± 0.28	2.64 ± 0.78	$\frac{1}{2}^+$	
	137.5 ± 0.7	1.18 ± 0.29	3.17 ± 0.78	$\frac{1}{2}^+$	
	147.2 ± 0.8	3.55 ± 0.51	9.25 ± 1.33	$\frac{1}{2}^+$	
	163.0 ± 0.9	0.53 ± 0.11	1.32 ± 0.27	$\frac{1}{2}^+$	
	172.5 ± 1.0				
Fe^{56}	-2.0		3.96	$\frac{1}{2}^+$	$\Gamma_\gamma = 0.64$ eV
	27.66 ± 0.10	1.52 ± 0.04	9.14 ± 0.24	$\frac{1}{2}^+$	
	73.90 ± 0.30	0.54 ± 0.07	1.98 ± 0.26	$\frac{1}{2}^+$	
	83.60 ± 0.40	1.03 ± 0.08	3.57 ± 0.28	$\frac{1}{2}^+$	1.88 ± 0.94
	122.50 ± 0.60	0.014 ± 0.005	0.04 ± 0.014	$\frac{1}{2}^+$	
	129.60 ± 0.60	0.66 ± 0.10	1.84 ± 0.28	$\frac{1}{2}^+$	
	139.90 ± 0.80	2.27 ± 0.20	6.08 ± 0.54	$\frac{1}{2}^+$	
	168.7 ± 1.0	0.76 ± 0.11	1.85 ± 0.27	$\frac{1}{2}^+$	
	187 ± 1.0	3.20 ± 0.23	7.40 ± 0.53	$\frac{1}{2}^+$	
Fe^{57}	6.280 ± 0.010	2.4 ± 0.1	30.28 ± 1.26		

should be noted that only strong levels have been included in this analysis and many weak observed levels have been omitted. The indicated mean s-wave level spacings are thus upper limits. The actual spacing is probably smaller. The measured s-wave strength functions to 200 keV are $S_0 = (3.2 \pm 1.6) \times 10^{-4}$ for Fe^{54} and $S_0 = (1.88 \pm 0.95) \times 10^{-4}$ for Fe^{56}. The values of the channel radius R and the coefficients A_J and B_J used in the analysis are given in Table III.

C. Nickel

Solid metal plates and sheets of the natural element of thicknesses $n^{-1} = 4.30$, 17.26, and 67.73 b/atom were used for the measurements. The observed total-cross-section-vs-energy curves are shown in Figs. 6(a)–6(c) and resonance energies are listed in Table V. The detailed experimental curves over a wider energy interval are given elsewhere.[4,5] The data shown in the present figures involve some multichannel averaging which removes some of the weak levels which were present in the data but were not analyzed in this study. The averaging was not done where sharp structure of the stronger levels were present. The cross-section curves show multiple structure near many broad resonances. Since natural nickel contains many isotopes with masses 58, 60, 61, 62, and 64 in varying abundances as noted earlier, it is not surprising to see this complicated resonance structure. The total-cross-section measurements of natural as well as separated isotopes of masses 58 and 60 have been previously made by Bilpuch *et al.*[12] From their measurements it is evident that most of the resonances in the two isotopes occur at about the same neutron energies, which is rather surprising in view of the different excitation energies of the two compound nuclei involved. This effect, however, complicates the analysis of the data.

The very broad resonance at 4.16 keV can only be assigned to Ni^{62} on the basis of the observed peak cross section in our measurement. The earlier Duke data threw some doubt on this isotopic assignment on the basis of their observed cross section; however, we have a unique assignment for this resonance to the isotope of Ni^{62} with parameters $E_0 = 4540$ eV, $\Gamma_n = 1350$ eV. Our value of neutron width is very different from the value quoted by Bilpuch *et al.*[12] but is in good agreement with the area-analysis measurement of Pawlicki, Smith, and Thurlow.[19]

The theoretical fit to the low-energy and thermal cross-section data can be obtained by taking into consideration a negative resonance, since the cross section rises at low energies. The resonance parameters given in Table V reproduce

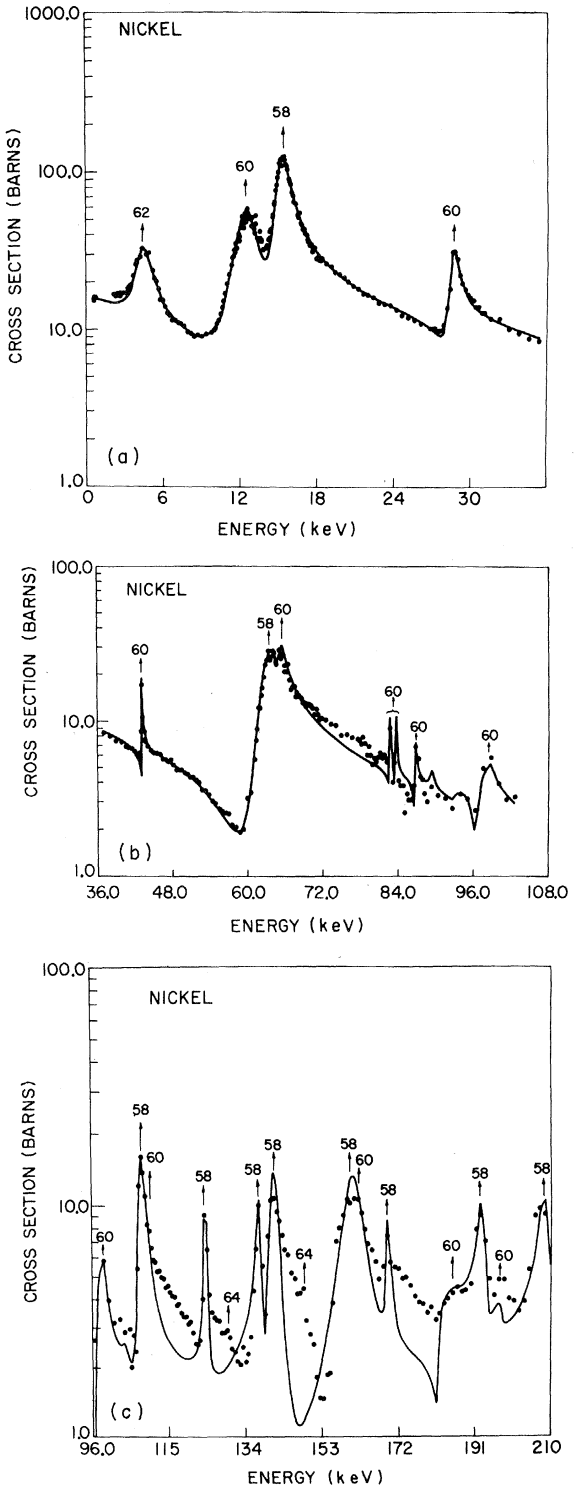

FIG. 6. (a)–(c) The observed neutron total cross section in natural nickel in the energy region up to 210 keV. The data have been averaged over many channels in between the resonance structure and on the resonance peaks when the peaks are much broader than the instrumental resolution. The smooth curve is the R-matrix fit with the resonance parameters as given in Table V.

TABLE V. Parameters of resonances observed in natural nickel as determined by the R-matrix analysis of the neutron total cross section. The energies are given in the laboratory system.

	E_0 (keV)	Γ_n (keV)	Γ_n^0 (eV)	J^π	S_0 (units of 10^{-4})
Ni^{58}	−28.5	16.4 ±0.9	98.0 ±5.4	$\frac{1}{2}^+$	
	15.3 ±0.2	1.14 ± 0.03	9.23 ± 0.24	$\frac{1}{2}^+$	
	63.2 ±0.3	3.65 ± 0.33	14.52 ± 1.31	$\frac{1}{2}^+$	
	108.0 ±0.5	1.47 ± 0.17	4.47 ± 0.52	$\frac{1}{2}^+$	
	123.8 ±0.6	0.74 ± 0.20	2.10 ± 0.57	$\frac{1}{2}^+$	4.2 ±1.9
	137.5 ±0.7	1.76 ± 0.20	4.76 ± 0.54	$\frac{1}{2}^+$	
	140.5 ±0.8	3.46 ± 0.49	9.23 ± 1.31	$\frac{1}{2}^+$	
	159 ±1	7.38 ± 2.11	18.51 ± 5.29	$\frac{1}{2}^+$	
	169 ±1	0.87 ± 0.22	2.11 ± 0.53	$\frac{1}{2}^+$	
	192 ±1	4.05 ± 0.58	9.24 ± 1.32	$\frac{1}{2}^+$	
	207 ±1.5	6.03 ± 1.20	13.25 ± 2.64	$\frac{1}{2}^+$	
Ni^{60}	12.4 ±0.1	1.91 ± 0.06	17.16 ± 0.54	$\frac{1}{2}^+$	
	28.65 ± 0.05	0.69 ± 0.04	4.08 ± 0.24	$\frac{1}{2}^+$	
	43.1 ±0.1	0.14 ± 0.03	0.67 ± 0.15	$\frac{1}{2}^+$	
	65.3 ±0.2	0.81 ± 0.14	3.17 ± 0.78	$\frac{1}{2}^+$	
	82.8 ±0.3	0.11 ± 0.04	0.39 ± 0.14	$\frac{1}{2}^+$	3.5 ±1.4
	83.8 ±0.3	0.08 ± 0.04	0.29 ± 0.14	$\frac{1}{2}^+$	
	86.7 ±0.3	0.16 ± 0.04	0.53 ± 0.14	$\frac{1}{2}^+$	
	97.7 ±0.4	1.07 ± 0.16	3.42 ± 0.51	$\frac{1}{2}^+$	
	109.5 ±0.5	1.75	5.29	$\frac{1}{2}^+$	
	161 ±1	5.3 ±2.0	13.20 ± 5.00	$\frac{1}{2}^+$	
	186 ±1	5.7 ±2.3	13.22 ± 5.34	$\frac{1}{2}^+$	
	196 ±1	3.5 ±2.3	7.90 ± 5.20	$\frac{1}{2}^+$	
Ni^{62}	4.54 ± 0.05	1.34 ± 0.09	19.89 ± 1.34	$\frac{1}{2}^+$	
	89.3 ±0.35	0.25 ± 0.12	2.64 ± 0.40	$\frac{1}{2}^+$	2.68 ± 1.69
	95.5 ±0.40	1.62 ± 0.40	5.29 ± 1.31	$\frac{1}{2}^+$	
	104.5 ±0.5	3.85	11.90	$\frac{1}{2}^+$	
	148.5 ±0.8	0.20	0.53	$\frac{1}{2}^+$	

very good agreement with the coherent scattering cross section at thermal energy and with the total cross-section data over the entire energy region. In order to get agreement with the neutron-capture cross section at thermal energy it is necessary to assume a value of $\Gamma_\gamma = 9.0$ eV for the negative resonance which contributes mainly to this cross section. All the observed resonances contribute a very small amount to the thermal capture for an assumed value of $\Gamma_\gamma = 10$ eV.

A comparison of the calculated cross section for the resonance parameters given in Table V, with the observed cross section is shown in Figs. 6(a)–6(c). The agreement is quite good in general except in between resonances at higher energies. This may be due to either the presence of unresolved p-wave resonances in the main isotopes of masses 58 and 60 or s-wave resonances in Ni^{62} and Ni^{64}. The high cross section at the high-energy end of resonances at 140 keV may be due to inadequate subtraction of cross section due to aluminum resonances which are present in the open beam.

The cross section of nickel separated isotopes have more recently been performed by the Duke group[7] with better resolution from 50 to 650 keV. The values of the revised resonance energies in Ni^{58} are systematically lower than ours by about 1.5 keV, although their energies are in agreement with our values for Ni^{60}. Large differences in neutron widths have been noted for some resonances. They have also observed two new s-wave resonances in Ni^{58} at 136.5 and 167.5 keV in agreement with our observation.

The high-resolution keV neutron-capture and transmission measurements in Ni^{60} have been recently made by Stieglitz, Hockenbury, and Block.[20] Our resonance energies are in excellent agreement with their results, although some discrepancies in the neutron widths are present. In addition to the resonances listed in Table V, strong resonances have been observed at 216 ± 1, 235 ± 1.5, 258 ± 1.8, 274 ± 2, 282 ± 2, 294 ± 2, 317 ± 2.5, 327 ± 2.5, and 333 ± 2.5 keV. Many weak levels have also been observed at 32.2 ± 0.08, 36.1 ± 0.1, 47.9 ± 0.15, 60.7 ± 0.2, and 133.2 ± 0.7 keV.

The mean level spacing of the various isotopes of nickel of masses 58, 60, and 62 are 22 ± 4, 20 ± 3, and 30.0 ± 5 keV, respectively. The corresponding strength functions for these nuclei are

$(4.2 \pm 1.9) \times 10^{-4}$, $(3.5 \pm 1.4) \times 10^{-4}$, and $(2.68 \pm 1.69) \times 10^{-4}$, respectively.

Level-Spacing Distribution

In the past few years considerable theoretical and experimental interest has developed in determining the law of distribution of level energies in complex nuclei. A detailed investigation[3] of the distribution of spacings between levels of heavy nuclei definitely established the effect of repulsion between levels and also showed that the distribution was in reasonable agreement with that predicted by the random matrix model.[21-23] Hence it was considered interesting to see if the same distribution holds good for the intermediate-mass nuclei. However, the level structure of the intermediate-mass nuclei investigated here differs from that of heavy nuclei in that the number of levels observed in each of the even-even nuclei is very small and thus does not provide a good statistical sample for comparison with the theory when each nucleus is treated separately. For a reliable comparison of the experimental results with the theoretical distribution it is essential that the instrumental resolution be good enough to resolve all the levels. For this reason the maximum energy for which levels were considered resolved was chosen where the resolution (ΔE) was less than one tenth the mean level spacing. Hence the levels analyzed were limited to 200-keV energy, although level structure has been observed up to much higher energies. Since the number of levels observed up to these energies in each of these nuclei was small, the separate $l=0$ level-spacing distribution for each nucleus was computed and the results were combined to provide a better statistical sample.

The combined results obtained for the ($I=0$) nuclei Ti^{48}, Fe^{54}, Fe^{56}, Ni^{58}, Ni^{60}, and Zn^{64} are shown in Fig. 7. The theoretical distribution of Wigner[21] and that of the random distribution are also shown for comparison. Figure 8 shows the results for next-nearest spacing distribution of the combined $I=0$ nuclei and is compared with the Porter-Kahn[22,23] theoretical distributions and that of the purely random distribution.

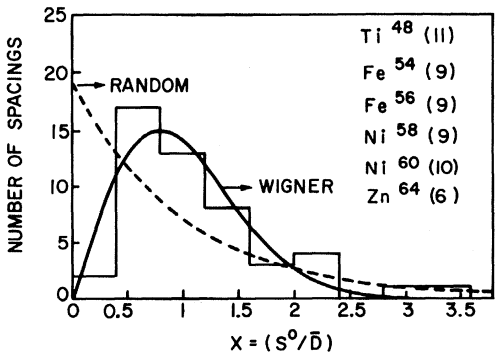

FIG. 7. Combined nearest-neighbor level-spacing distribution of the even-even nuclei Ti^{48}, Fe^{54}, Fe^{56}, Ni^{58}, Ni^{60}, and Zn^{64}. The smooth curve is the Wigner distribution and the broken curve is the random distribution of energy levels.

The level-repulsion effect is clearly evident in these results. The nearest-neighbor spacing distribution is in general agreement with the Wigner shape which is based on the random matrix model. The two largest observed spacings are not compatible with the Wigner shape and probably indicate missed s-wave levels in these energy intervals. The random distribution is clearly not in agreement with the data.

In the comparison of the next-nearest-neighbor spacing distribution with the two theoretical choices, the random matrix model (Porter-Kahn) is again in relatively good agreement with the data except for the two largest spacings. This merely confirms that a few weak $l=0$ resonances were probably missed.

The correlation coefficient between adjacent level spacings has also been measured for the levels of the separated isotopes of ^{48}Ti, ^{54}Fe, ^{56}Fe, ^{60}Ni, and ^{58}Ni and these values with the number of levels observed and the mean spacing are shown in Table VI. The theoretical value calculated by Porter for 3×3 matrices is also shown. These results show a slightly stronger correlation than the theoretical value. However, the results are not inconsistent with the theoretical value within the accuracy of the measurements. The relatively large values of the correlation coefficient can also arise from the very small number of levels analyzed in each case.

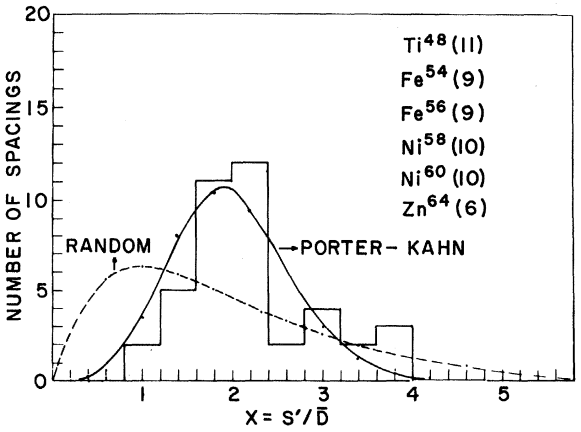

FIG. 8. Combined next-nearest-neighbor level-spacing distribution. The smooth curve is that calculated by Porter and Kahn for a random-matrix model and the broken curve is that of random occurence of level energies.

TABLE VI. The measured values of the correlation coefficient of adjacent spacings of levels of nuclei Ti^{48}, Fe^{54}, Fe^{56}, Ni^{58}, and Ni^{60}.

Target nucleus	Spin	Maximum energy (keV)	No. of levels observed	$\langle D \rangle$ (keV)	Spacing correlation coefficient
Ti^{48}	0	200	11 [a]	18±3	−0.45±0.27
Fe^{54}	0	200	10	20±4	−0.36±0.20
Fe^{56}	0	225	9	25±5	−0.42±0.21
Ni^{58}	0	200	9	22±4	−0.54±0.25
Ni^{60}	0	200	10	20±4	−0.48±0.29
Theoretical 3×3 matrices					−0.254

[a]This includes the levels at 74.2, 133.0, and 185 keV which could possibly be p wave.

Even if there were no true covariance ≠0 phenomena present, one expects to obtain a negative sample covariance $\approx -1/n \pm (1/n)^{1/2}$, where n is due to the bias of using the sample mean value rather than the "true population mean value." An extreme example is when only two unequal values are present experimentally. The calculated covariance is then always exactly −1.0.

Note added in proof: After the submission of our paper to the *Physical Review*, we received a communication from Dr. Seth of Northwestern University that comparable work on $Ti^{48,49}$ isotopes has been performed at Karlsruhe by Muller and Rohr and has been submitted for publication. There appears to be good agreement of our results with theirs for these isotopes.

ACKNOWLEDGMENTS

We would like to express our sincere thanks to J. S. Petersen for his active participation in some of these measurements. The technical assistance rendered by the velocity-selector technicians A. Blake, J. Spiteri, S. Marshall, and D. Ryan and other members of the Nevis cyclotron operating staff are gratefully acknowledged. E. Ham and U. N. Singh helped in the data analysis.

*Work supported in part by the National Science Foundation.

†Work supported in part by the U. S. Atomic Energy Commission.

[1]H. H. Barshall, Phys. Rev. 86, 431 (1952).

[2]H. Feshbach, C. E. Porter, and V. Weisskopf, Phys. Rev. 96, 448 (1954).

[3]J. L. Rosen, J. S. Desjardins, J. Rainwater, and W. W. Havens, Jr., Phys. Rev. 118, 687 (1960), U^{238} – I; J. S. Desjardins, J. L. Rosen, W. W. Havens, Jr., and J. Rainwater, *ibid.* 120, 2214 (1960), Ag, Au, Ta – II; J. B. Garg, J. Rainwater, J. S. Petersen, and W. W. Havens, Jr., *ibid.* 134, B985 (1964), Th^{232}, U^{238} – III; J. B. Garg, W. W. Havens, Jr., and J. Rainwater, *ibid.* 136, B177 (1964), As, Br–IV; J. B. Garg, J. Rainwater, and W. W. Havens, Jr., *ibid.* B547 (1965), Nb, Ag, I, Cs – V; S. Wynchank, J. B. Garg, W. W. Havens, Jr., and J. Rainwater, *ibid.* 166, 1234 (1968), Mo, Sb, Te, and Pr – VI.

[4]J. B. Garg, J. Rainwater, and W. W. Havens, Jr., University of Columbia Report No. EANDC(US) 54 "L" C 1860, 1964 (unpublished). These data are available from the National Neutron Cross Section Center at Brookhaven National Laboratory.

[5]*Neutron Cross Sections*, compiled by M. D. Goldberg, S. Mughabghab, B. A. Magurno, and V. M. May, Brookhaven National Laboratory Report No. BNL 325 (U. S. Government Printing Office, Washington, D. C., 1964), 2nd ed., Suppl. No. 2.

[6]J. Rainwater, W. W. Havens, Jr., and J. B. Garg, Rev. Sci. Instr. 35, 263 (1964); J. Hahn and W. W. Havens, Jr., *ibid.* 31, 490 (1960).

[7]J. A. Farell, E. G. Bilpuch, and H. W. Newson, Ann. Phys. (N.Y.) 37, 367 (1966).

[8]H. Feshbach, D. C. Peaslee, and V. Weisskopf, Phys. Rev. 71, 145 (1947).

[9]E. Wigner and L. Eisenbud, Phys. Rev. 72, 29 (1947).

[10]A. M. Lane and R. G. Thomas, Rev. Mod. Phys. 30, 257 (1958).

[11]F. W. K. Firk, J. E. Lynn, and M. C. Moxon, Proc. Phys. Soc. (London) 82, 477 (1963).

[12]E. G. Bilpuch, K. K. Seth, C. D. Bowman, R. H. Tabony, R. C. Smith, and H. W. Newson, Ann. Phys. (N.Y.) 14, 387 (1961).

[13]W. M. Good, D. Paya, R. Wagner, and T. Tamura, in *Proceedings of the International Conference on the Study of Nuclear Structure, Antwerp, Belgium, 1965* (North-Holland Publishing Company, Amsterdam, The Netherlands, 1966).

[14]C. G. Shull, M. K. Wilkinson, and M. H. Mueller, Phys. Rev. 118, 797 (1960).

[15]C. T. Hibdon, Phys. Rev. 108, 414 (1957).

[16]H. W. Newson, E. G. Bilpuch, F. P. Karriker, L. W. Weston, J. R. Patterson, and C. D. Bowmann, Ann. Phys. (N.Y.) 14, 365 (1961).

[17]J. A. Moore, H. Palevsky, and R. E. Chrien, Phys. Rev. 132, 801 (1963).

[18]C. D. Bowman, E. G. Bilpuch, and H. W. Newson, Ann. Phys. (N.Y.) 17, 319 (1962).

[19]G. S. Pawlicki, E. C. Smith, P. E. F. Thurlow, Oak Ridge National Laboratory Report No. ORNL-1496, 1952 (unpublished).

[20]R. G. Stieglitz, R. W. Hockenbury, and R. C. Block, private communication.

[21]E. P. Wigner, Oak Ridge National Laboratory Report No. ORNL-2309 (unpublished), p. 59.

[22]C. E. Porter, Nucl. Phys. 40, 167 (1963).

[23]P. B. Kahn, Nucl. Phys. 41, 159 (1963).